ResearchGate

See discussions, stats, and author profiles for this publication at: https://www.researchgate.net/publication/276399906

Four-order stiffness variation of laser-fabricated photopolymer biodegradable scaffolds by laser parameter modulation

ARTICLE *in* MATERIALS SCIENCE AND ENGINEERING C · MAY 2015

Impact Factor: 3.09 · DOI: 10.1016/j.msec.2015.05.054

CITATIONS
3

READS
64

6 AUTHORS, INCLUDING:

Luca Ceseracciu
Istituto Italiano di Tecnologia
46 PUBLICATIONS **380** CITATIONS
SEE PROFILE

Alberto Diaspro
Istituto Italiano di Tecnologia
499 PUBLICATIONS **5,469** CITATIONS
SEE PROFILE

Szabolcs Beke
Istituto Italiano di Tecnologia
36 PUBLICATIONS **318** CITATIONS
SEE PROFILE

All in-text references underlined in blue are linked to publications on ResearchGate, letting you access and read them immediately.

Available from: Szabolcs Beke
Retrieved on: 25 January 2016

Materials Science and Engineering C 55 (2015) 14–21

Contents lists available at ScienceDirect

Materials Science and Engineering C

journal homepage: www.elsevier.com/locate/msec

Four-order stiffness variation of laser-fabricated photopolymer biodegradable scaffolds by laser parameter modulation

Balázs Farkas [a], Ilaria Romano [a], Luca Ceseracciu [a], Alberto Diaspro [a], Fernando Brandi [a,b], Szabolcs Beke [a,*]

[a] Department of Nanophysics, Istituto Italiano di Tecnologia (IIT), Via Morego 30, 16163 Genova, Italy
[b] Istituto Nazionale di Ottica, Via Moruzzi 1, 56124 Pisa, Italy

ARTICLE INFO

Article history:
Received 23 October 2014
Received in revised form 30 March 2015
Accepted 17 May 2015
Available online 21 May 2015

Keywords:
Stereolithography
Excimer laser
Biodegradability
Poly(propylene fumarate)
Scaffolds

ABSTRACT

The effects of various fabrication parameters of our Mask Projection Excimer Laser StereoLithography (MPExSL) system were investigated. We demonstrate that laser parameters directly change the physical properties (stiffness, thermal degradation, and height/thickness) of the poly(propylene fumarate) (PFF) scaffold structures. The tested parameters were the number of pulses, fluence per pulse and laser repetition rate. We present a four-order tuning capability of MPExSL-fabricated structures' stiffness without altering the resin composition or using cumbersome post-treatment procedures. Thermogravimetric analysis and differential scanning calorimetry confirmed this tuning capability. Prototype-segmented scaffold designs are presented and analyzed to further expand the concept and exploit this in situ stiffness tuning capability of the scaffolds for tissue engineering and regenerative medicine applications.

© 2015 Published by Elsevier B.V.

1. Introduction

Tissue engineering (TE) [1–4] is an expanding interdisciplinary field with the purpose of growing tissues directly on controlled microenvironments called scaffolds. The design and fabrication of structures are among those parameters that strongly affect the successful outcome of tissue formation. Therefore, before these artificial structures can be considered for medical applications, they must fulfill some general requirements, such as proper porosity and mechanical properties, making them capable of supporting the engineered tissue [5].

One of the major goals of tissue engineering is to provide a rapid and reliable production of well-designed and functional scaffolds, capable of fulfilling the aforementioned requirements. The tuning of these characteristics is also highly desired — in some cases, even within the same structure, in order to achieve multi-phase constructs [6,7].

It is therefore crucial to be able to reliably adjust all physical parameters of the scaffolds, including the stiffness (Young's modulus), the degradation (rate), and the geometry (size and porosity) with a high level of biocompatibility. All structures presented here were fabricated by our novel fabrication process called Mask Projection Excimer Stereolithography (MPExSL) [8] using poly(propylene fumarate) (PFF) resin.

MPExSL is a simple and highly efficient method optimized for rapid prototyping of single-layer (2D) and multilayer (3D) TE scaffolds of various sizes and porosities. It is based on pulsed excimer laser photocuring of a biocompatible photosensitive resin. The biocompatibility of MPExSL-fabricated structures has already been investigated by our group in previous in vitro [9] and in vivo [10] studies. Besides, elastine [11,12] and titanate nanotubes [13,14] were utilized as functional coatings on these PPF scaffolds.

MPExSL applies several variable laser parameters — such as the number of pulses, the pulse fluence and laser repetition rate. The main resin composition parameter is the photoinitiator concentration [15–18]. All of these parameters are potentially capable of tuning the physical properties of the scaffolds [19] due to the changes in the initial photocross-linking density [16], and the reversion occurring under intense exposure [20]. The current study aims at unraveling the effects of these aforementioned parameters on the height, thermal degradation, and stiffness of the fabricated structures.

Scaffolds with properly adjusted stiffness are indispensable to mimic the tissue's extracellular matrix [21–24]. High stiffness is also important for greater structural integrity, for instance, in osteochondral tissue regeneration [25–27]. Usually though, the stiffness tuning capability of these scaffolds is limited, leading to constructs fabricated from various metals, polymers, and ceramics, depending on their functionality. The lack of a facile tuning process becomes apparent when tissue interfaces are repaired using composite scaffolds [25–29] and these structures are made of multiple materials employing lengthy and costly processes.

In this study, we present an *in situ*, 4-order stiffness tuning (4 MPa to 4 GPa) of biodegradable and biocompatible scaffolds without altering the PPF resin composition. The modulation of the scaffold's degradation rate by hydrolysis in 37 °C DMEM is also reported.

* Corresponding author at: Department of Nanophysics, Italian Institute of Technology, Via Morego 30, 16163 Genova, Italy.
E-mail address: szabolcs.beke@iit.it (S. Beke).

http://dx.doi.org/10.1016/j.msec.2015.05.054
0928-4931/© 2015 Published by Elsevier B.V.

All samples were fabricated by our fast prototyping MPExSL system/technique.

2. Materials and methods

2.1. Stereolithography setup and mask projection

In MPExSL, schematically illustrated in Fig. 1, the image of a mask is projected on the liquid resin defining the geometry of the solidified polymer scaffold. The pulse fluence is controlled by a variable attenuator, while the proper positioning of the resin surface is performed by moving the x-, y-, z-axes using a motorized 3-axis stage. The precise stage movement, the repetition rate and the number of pulses are controlled by a personal computer. A CCD camera is mounted on the top of the optical system to in situ monitor the process.

For 2D scaffold production, a thin layer of resin is sandwiched between a glass holder and a quartz plate as presented in [30].

For 3D scaffolds, the thickness of one layer depends on the energy absorbed in the resin during the exposure time, i.e., the combination of number of pulses, fluence per pulse, repetition rate, light wavelength, and photoinitiator concentration. The overlap between the scaffold building layers is adjusted by a fourth axis, moving the stage vertically in the resin between laser exposures.

A set of interchangeable masks is applied to define the dimensions, porosity, and shape of the fabricated structures. The high-resolution features that can be achieved by our projection technique are demonstrated in Fig. 2a. For 2D scaffolds, in principle, pore diameters can be as low as 5 μm. For 3D structures, due to differences in the fabrication technique meaning the layer-by-layer method and the ordinarily high aspect ratio, some tens of μm in diameter can be achieved depending on the scaffold height. The outer diameter/geometry of the scaffold can be further modulated by an iris positioned in the beam path right in front of the mask(s).

Certain flexibility emerges from the programmable feature of the MPExSL's XYZ stage control illustrated in Fig. 2b, where a “star” shape was used as a standard unit for the fabrication.

2.2. The applied resin and light source

Poly(propylene fumarate) (PPF) [31–33] is a good and versatile candidate for tissue engineering due to its (i) biodegradability, (ii) cytocompatibility of the degradation products, (iii) high Young's modulus and (iv) the unsaturation in the backbone of the polymer.

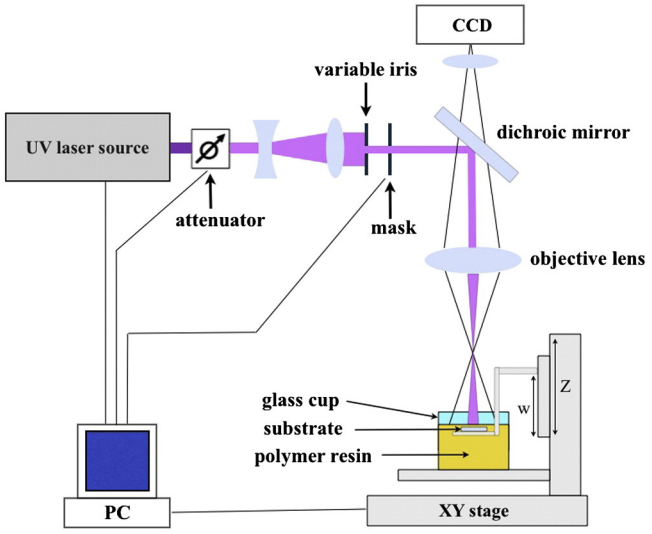

Fig. 1. Schematic of the MPExSL setup for 3D scaffold fabrication.

Pure PPF scaffolds can also be fabricated, albeit at the expense of time due to its high viscosity. In order to attain a high enough fabrication speed with MPExSL, the PPF viscosity has to be decreased. This is achieved by blending the PPF with diethyl(fumarate) (DEF) in a 7:3 weight/weight ratio.

The photocross-linking density is tuned by photoinitiator phenylbis (2,4,6-trimethylbenzoyl) phosphine oxide (BaPO) concentration.

It is important to note that since the light absorption of both the resin and the photoinitiator varies with the wavelength [30], the applied wavelength determines the curing (penetration) depth of the laser pulses into the polymer, thus the time needed for the fabrication of constructs. Compared to the 248-nm-light (KrF excimer laser), the 308 nm has a far greater penetration depth in the PPF resin, which results in a higher scaffold production capacity [30]. For this reason, in MPExSL a XeCl excimer laser operating at 308 nm is used (energy per pulse 70–260 mJ, pulse duration 20 ns, repetition rate 1–100 Hz).

All reagents and materials were purchased from Sigma-Aldrich and used as received.

2.3. Mechanical and thermal testing, FTIR

Stiffness measurements in both 2D and 3D were performed by means of nanoindentation on non-porous samples. The indenter was a Micro Materials Ltd. NanoTest, tests were conducted by using a Berkovich-tip with a maximum load of 0.6 mN, a dwell time at maximum load of 30 s, loading and unloading periods of 30 s and 15 s, respectively. Every sample has been measured at 16 different points (in a matrix of 4 × 4, distance between measurements 50 μm). Young's modulus was calculated through the Oliver and Pharr method each time. The stiffness for the whole sample was acquired eventually by having the mean value of these aforementioned 16 points. It is important to note that this nanoindentation setup (with the Berkovich-tip) could not be reliably used on samples with stiffness less than 4–5 MPa or when there was adhesion between the tip and the sample. Height measurements were carried out by a Veeco Dektak 150 profiler.

Thermogravimetric analysis (TGA) was conducted in a TGA Q500 from TA Instruments. The sample was placed in a platinum pan with an equilibrating step at 30 °C. Heating went to 800 °C with a 10 °C/min rate. Nitrogen flow was 50 ml/min.

PerkinElmer Diamond DSC was used for differential scanning calorimetry (DSC). In an aluminum pan, the sample was heated from −40 °C to 120 °C with 20 °C/min ramp, followed by a cool down with the same rate and a 5 min hold step at −40 °C. This was preferable so as to eliminate any thermal history on the samples. The temperature hold step was succeeded by a ramp-up process with the same parameters as before. Nitrogen gas flow was 20 ml/min.

Fourier transformed infrared spectroscopy (FTIR) was conducted using a Bruker Vertex 70v.

3. Results and discussion

In order to test the effects of different parameters, first 2D (i.e. single-layers) structures have to be characterized (Section 3.1). They are the basic building blocks of 3D structures and thus a good control over their properties is essential to successfully build uniform and stable multilayer constructs. Fundamental correlations of the light-polymer interaction presented in detail later in this article could already be observed here.

It is important to note the existing disparity between the 2D/sandwiched and the 3D/stereolithography processes though. In 2D, the quartz sheet diffracts a portion of the incoming laser pulse, resulting in a thin, partially-cured layer covering both the quartz and the sample. This low stiffness film can alter all nanoindentation measurements conducted on single-layers, preventing a reliable comparison to any 3D sample considering the mechanical properties. Thus, 3D structures

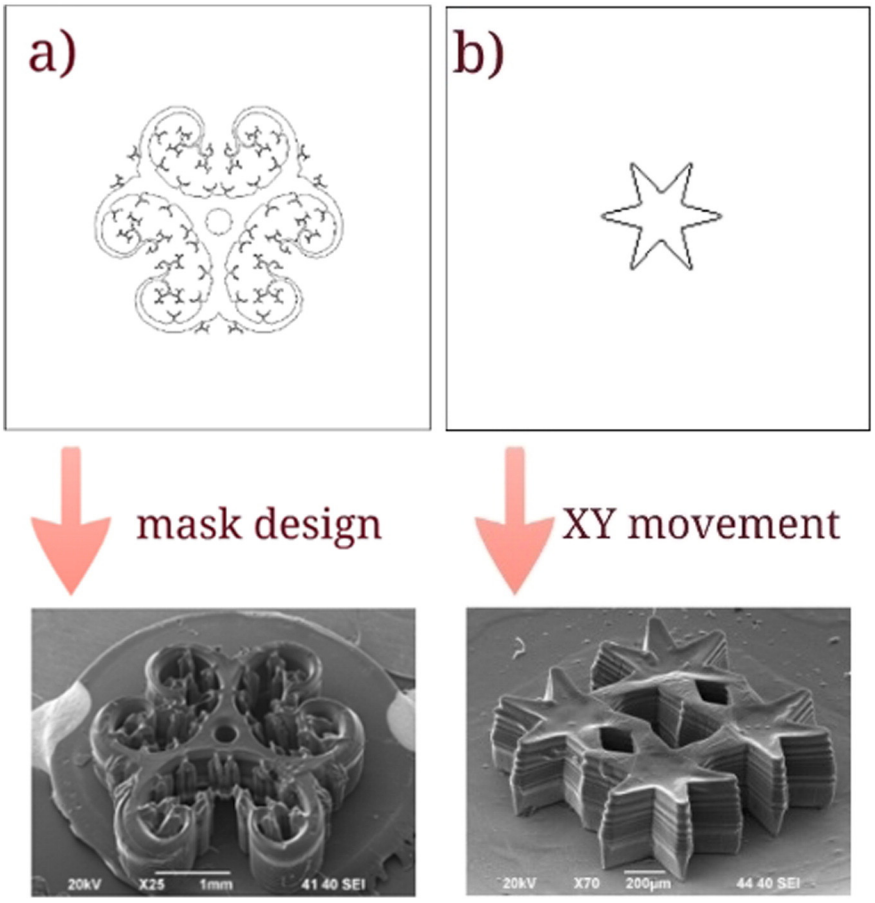

Fig. 2. Different scaffold designs demonstrating the broad capabilities of the mask projection technique: fine details (a); block building (b).

had to be fabricated and measured separately (Section 3.2), rendering most mechanical data acquired with 2D scaffolds.

3.1. Characterization of single-layers (films)

The thickness/height of a polymerized layer and the mechanical properties [9] can be tuned with the applied total fluence (fluence per pulse multiplied by the number of pulses) and the BaPO concentration. Thus, a map (Fig. 3) is beneficial to display proper and efficient control over the physical properties of the layers building up the desired 3D scaffolds.

Non-porous single-layers (films) were fabricated using a repetition rate of 50 Hz and a total fluence varied by the fluence per pulse (Fig. 3a). The applied numbers of pulses were 50, 124, 248, 336, 480, 720 and 1000. Minor decrease in the layer thickness is observed with increased repetition rates (Fig. 3b). On both Fig. 3a and b, the red line corresponds to the same 50 Hz, 10 mJ/cm^2 recipe for both graphs. Fig. 3a inset shows the layer thickness as a function of the fluence per pulse when the number of pulses is kept constant at 480. Not only the above mentioned laser parameters have effects on the layer thickness, but this tuning range is also strongly dependent on the resin's photoinitiator concentration, as presented in Fig. 3c. Three different BaPO concentrations (0.3% w/w, 0.6% w/w and 1% w/w) have been chosen and measured with single-layers fabricated when using a constant repetition rate of 50 Hz and fluence per pulse of 10 mJ/cm^2. The applied numbers of pulses were again 50, 124, 248, 336, 480, 720 and 1000. As expected, the layer thickness increases with lower BaPO concentrations due to lower absorption [30]. Similarly, less BaPO also resulted in softer scaffolds due to the photo-crosslinking mechanism [34].

Some changes in the stiffness have also been detected on these aforementioned 2D samples as well, fabricated by the same amount of photoinitiator. A simple comparison was performed using the recipe of 1% w/w BaPO concentration, 480 pulses, 50 Hz and 10 mJ/cm^2 fluence per pulse, using the 1% BaPO samples. The observations are summarized in Fig. 3d. It shows that layers fabricated with 10 mJ/cm^2 fluence per pulse and 5 Hz repetition rate have about 4-times higher Young's modulus (250–300 MPa) than the ones prepared with 50 Hz (75–100 MPa). When applying a repetition rate of 50 Hz and increasing the fluence up to 30 mJ/cm^2, the sample becomes too soft to be measured with the nanoindentation setup. Increasing the number of pulses from 480 to 1000 has negligible (less than 10%) effect on the stiffness.

3.2. Characterization of the laser parameters on 3D/multilayer structures

Relying on the preliminary results presented in Section 3.1, a set of experiments was conducted to map and prove the variation in the mechanical characteristics of the fabricated multilayer structures.

Apart from the total fluence, the product of the pulse fluence by the repetition rate was chosen as our second parameter, termed as 'energy flux density'.

3.2.1. Effects of the laser parameters on 3D scaffolds

The Investigation of the effect of the energy flux density was performed by fabricating a set of 2 mm-diameter, 5-layer, circular, non-porous scaffolds using 1% BaPO. For all multilayer structures, each layer was 100 µm thick with 20 µm overlaps, resulting in a 400 µm-high construct. (Of note, the layer thickness was selected to be constant 100 µm here, rather than the number of pulses. This was necessary to keep the fabrication efficiency high. After the discussion of Section 3.1, though, it is clear that the layer thickness will be adjusted by a combination of several laser parameters. To compensate the height-tuning effect of the various repetition rates and the fluences, the number of pulses

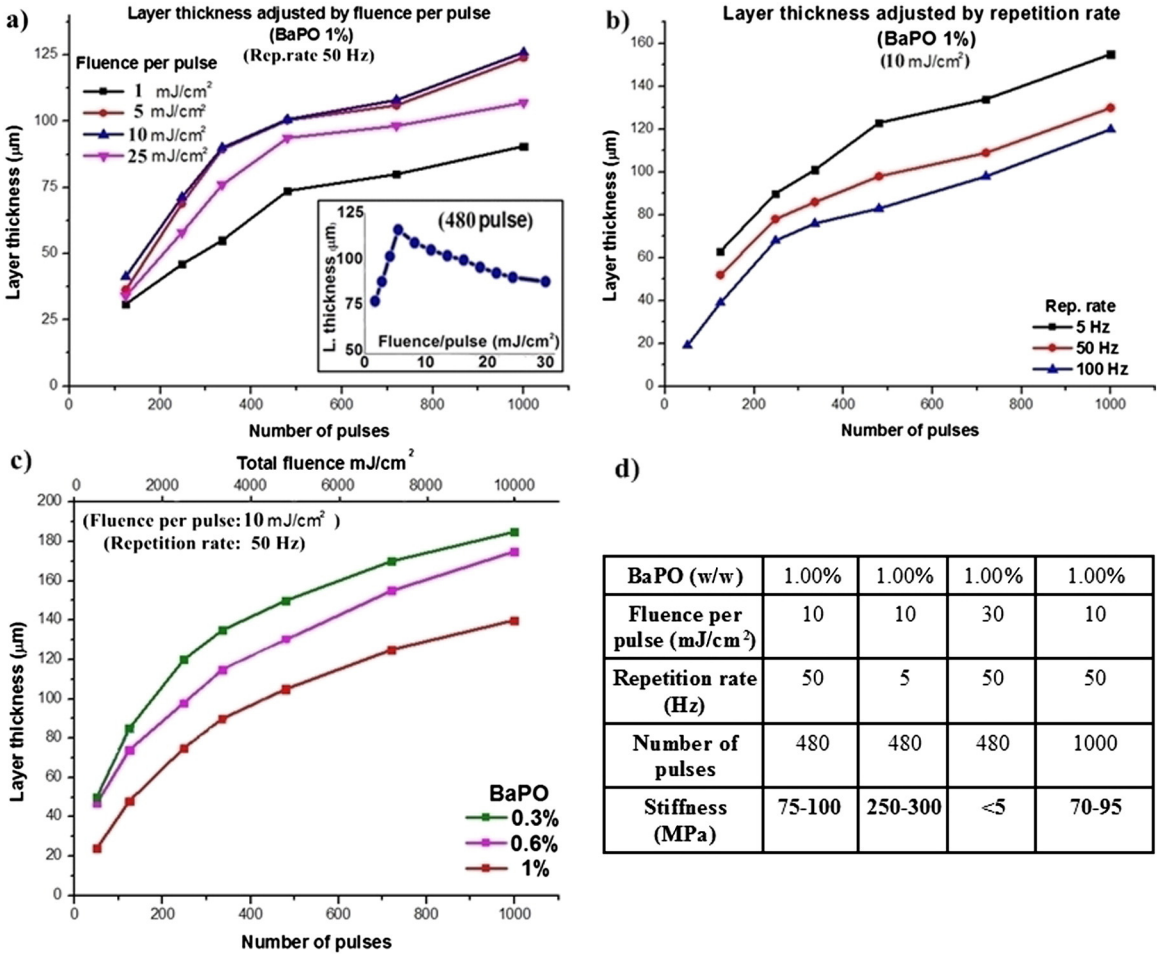

BaPO (w/w)	1.00%	1.00%	1.00%	1.00%
Fluence per pulse (mJ/cm²)	10	10	30	10
Repetition rate (Hz)	50	5	50	50
Number of pulses	480	480	480	1000
Stiffness (MPa)	75-100	250-300	<5	70-95

Fig. 3. Effects of laser parameters on single-layer thickness. All three parameters (fluence per pulse, repetition rate, number of shots) change the thickness. c) Effect of photoinitiator concentration on single-layer thickness. The layers become thicker under the effect of the same total fluence if there is less BaPO used. d) Effects of different laser parameters on single-layer stiffness. (For interpretation of the references to color in this figure legend, the reader is referred to the web version of this article.)

had to be adjusted accordingly. This was viable since changing of the number of pulses had negligible effect on the stiffness, as hinted in Section 3.1 and shown later in this section.)

We produced 72 constructs by applying repetition rates in the range of 1–100 Hz (in 8 steps) and fluences ranging from 2 to 30 mJ/cm^2 (in 10 steps) as presented in Fig. 4a. Fig. 4b and c present the measurement

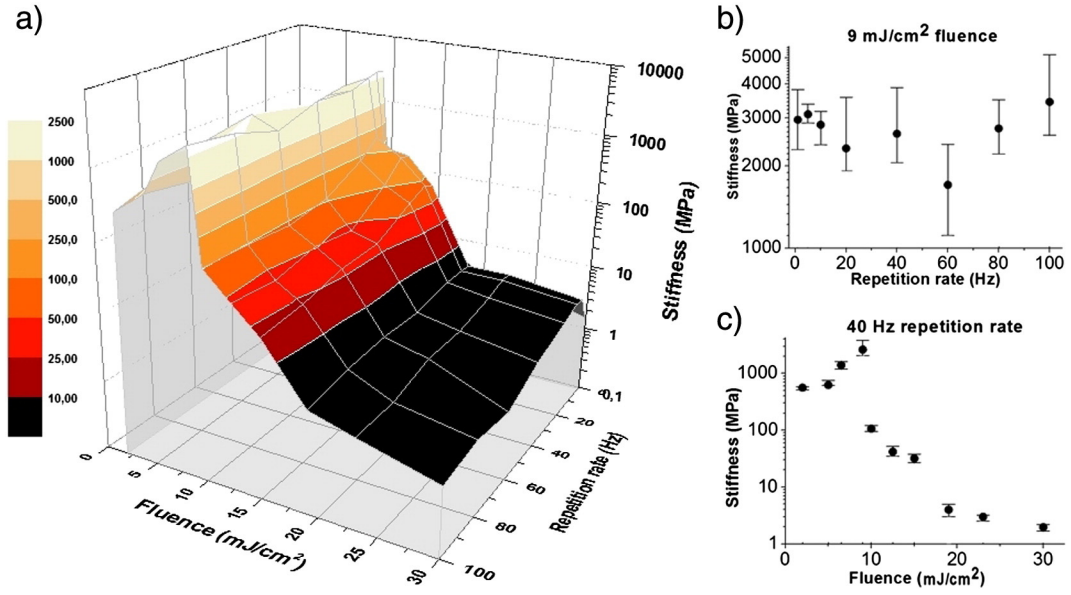

Fig. 4. a) Map of the tuning capability of the energy flux density. The stiffness shows linear increasing with the fluence, then decreases exponentially. The repetition rate scales with the stiffness only slightly. b and c present the measurement deviation for constant fluence (9 mJ/cm^2) and constant repetition rate (40 Hz), respectively.

deviation for constant fluence (9 mJ/cm^2) and constant repetition rate (40 Hz), respectively.

Fig. 4 shows that for fluence < 10 mJ/cm^2, the stiffness increases linearly with the fluence. This rise is from a few hundreds of MPa to a few GPa. After the fluence exceeds 10 mJ/cm^2, the stiffness starts to decrease exponentially, falling under 10 MPa when 20 mJ/cm^2 is reached. Regardless of this effect, the repetition rate presents a tuning capability as well: samples produced with 20 Hz tend to be multiple times stiffer than the ones built with 100 Hz or 1 Hz.

It is important to note that the lowest stiffness value cannot be precisely identified: all samples fabricated with fluences above 25 mJ/cm^2 were too soft to be reliably measured with the nanoindentation setup (i.e. most measurement points led to error messages due to low stiffness). The little data that was acquired with this setup had been processed, yet it is not possible to consider these anything but estimated values.

By observing the highest stiffness level of 4 GPa (at 10 mJ/cm^2 and 20 Hz) and the lowest accurate level of 4 MPa (at 25 mJ/cm^2 and 100 Hz), we achieved as high as a four-order difference in the stiffness without altering the resin composition. From empirical observations, it is highly plausible that applying greater fluences, this range could be further expanded. On the other hand, the observed lack of reliability might potentially be the marker of an imminent solid–gel transition of the photocured resin as well.

To test the other component of the total fluence (the number of pulses), 5-layer scaffolds were fabricated with 1% photoinitiator using 336, 480, 720, and 1000 pulses for each layer. 5 mJ/cm^2, 10 mJ/cm^2 and 20 mJ/cm^2 fluence per pulse were used with a repetition rate of 20 Hz.

It was observed that the number of pulses had no measurable effect on the stiffness under 10 mJ/cm^2 of fluence per pulse. With higher fluence though, a slight tuning capability was revealed. This tuning range was negligible compared to the repetition rate or the fluence per pulse.

Higher fluence with fewer pulses did not give the same stiffness value as lower fluence with more pulses, despite having the same amount of total fluence.

3.2.2. Thermal measurements

In order to better understand the structural mechanisms leading to the aforementioned tuning capability, some samples with highly different mechanical properties from Section 3.2.1 were investigated by TGA measurements, namely samples produced with fluence varying from 5 to 25 mJ/cm^2, repetition rate of 20 Hz.

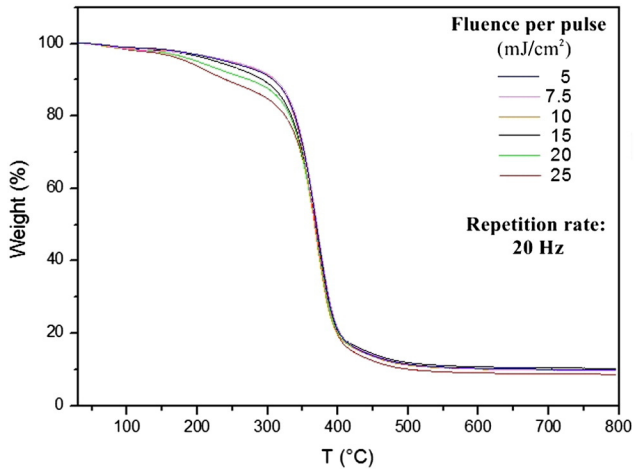

Fig. 5. TGA measurements on samples from Section 3.2.1. The softer the sample is, the earlier/lower temperature it starts to degrade.

The analysis shows a well noticeable trend among the samples (Fig. 5). The thermal behavior of all samples fabricated with less than 10 mJ/cm^2 fluence is identical, with a unique degrading temperature at around 370 °C. This suggests that the structure (chains length, crosslinks density) is basically the same. On the other hand, the steady drop in stiffness observed for fluences exceeding the threshold of 10 mJ/cm^2 can be explained by the visible earlier degradation, at around 200 °C, which is attributed to the presence of a second phase, probably composed by resin degraded by the high laser energy, as mentioned for thickness in Section 3.1.

DSC was conducted on selected samples, namely the softest (25 mJ/cm^2) and the stiffest (10 mJ/cm^2) ones, both fabricated at 20 Hz, with 480 pulses, 1% BaPO. The number of layers was 20 with overlaps of 20 μm.

Results showed little difference in the glass transition temperature, dropping from 39 °C for the stiffer sample to 29 °C for the softer one. This again proves the slight difference in the structure of the polymerized materials, probably due to the presence of a phase of degraded resin that loosen the polymeric network.

3.2.3. FTIR measurements

FTIR was conducted on pre-cured resin and scaffolds with highly varied stiffnesses in order to analyze the photocuring efficiency. Softer samples gave sharper peaks due to the better interaction between the material and the detector.

As presented in Fig. 6, the peaks mainly attributed to the C═C double bond (730 for C═C cis, 980 for RCH═RCH$_2$ and 1650 for C═C stretching) disappear in samples fabricated by fluences resulting in higher stiffness. This correlates well with the curing process.

A shift towards higher wavenumbers with the RC(═O)R′ ketone group peak can also be observed in scaffolds with high Young modulus. This may be connected to the rearrangement of the polymer chains also marking a greater curing efficiency and thus, higher stiffness.

Of note, no differences have been observed with 3D samples fabricated using the same fluence, but different repetition rates.

3.2.4. Discussion of tests conducted on multilayer structures

All results presented on 3D scaffolds are in accordance with the effects observed in 2D, meaning that the stiffness tuning capability is the function of the fluence per pulse and, to lesser extent, the repetition rate. The number of pulses on the other hand has negligible influence on the mechanical properties using the tested frequency/fluence values. We assume that the effects changing the stiffness properties (heat and crosslinking/fragmenting cycle) reach equilibrium in only a couple of pulses.

Considering the fluence per pulse, using less than 10 mJ/cm^2 the stiffness scaling is purely due to the crosslinking density. Surpassing this fluence level increases the chance of the already-linked chains to fragment, thus decreasing the overall stiffness. This theory is supported by the FTIR measurements where the C═C double bonds reappear in the high-fluence/soft samples. Furthermore, the DSC and TGA measurements show disparity in the glass transition temperature and two degradation temperatures, respectively.

Similarly, we theorize that the effect of repetition rate on the final microstructure is connected to thermal diffusion effects, by affecting the temperature reached within the sample: crosslinking density slightly increases with repetition rate, as energy dissipation becomes lower, then a threshold for chains degradation is reached and mechanical properties are affected negatively.

3.3. Utilizing the tuning capability

The applied laser pulse fluence in combination with the repetition rate can be used to tune both 2D and 3D MPExSL scaffolds' stiffness in the order of four (from a few MPa to a few GPa). Prototype 3D-

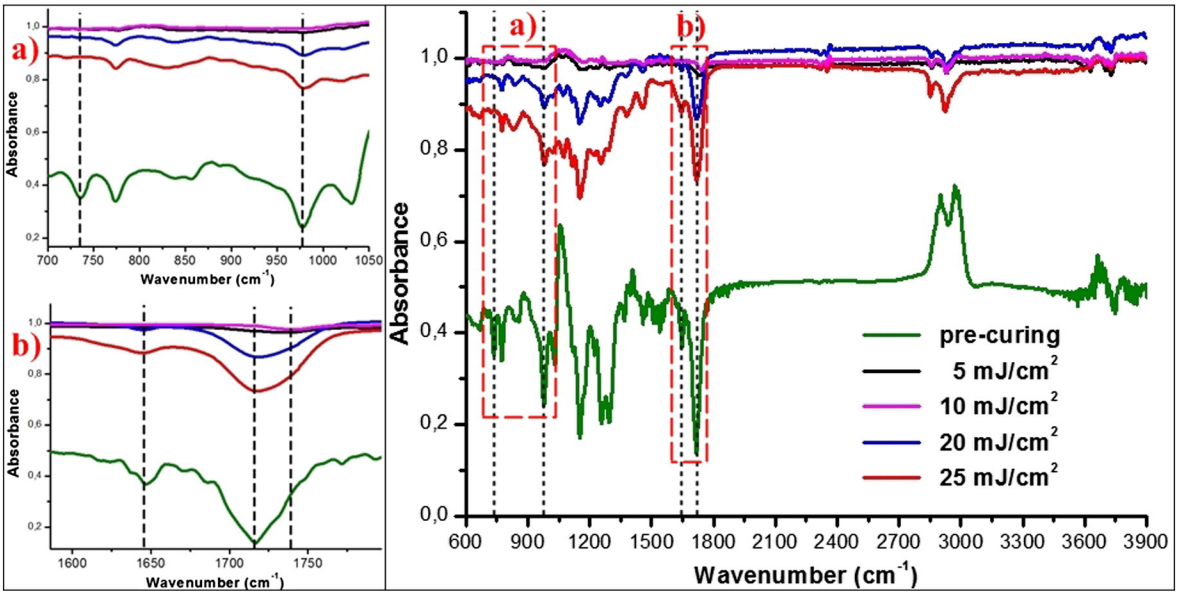

Fig. 6. FTIR analysis of samples fabricated by different fluences. a, b show the close-ups of two different regions of the main spectrum.

segmented scaffolds were constructed to show the utility of this tuning in the fabrication of multilayer structures.

3.3.1. Mimicking composite scaffolds

Two constructs were built mimicking the mechanical properties of composite scaffolds. Two 0.5 mm-wide concentric rings (with inner diameters of 2 and 3 mm) were fabricated around a central cylindrical core (diameter of 2 mm), resulting in a 3-segment, non-porous, circular block, as presented in Fig. 7. The two constructs were identical: both constructs had 25 layers, with a layer thickness of 100 μm and layer overlap of 20 μm, 1% BaPO.

Nanoindentation was conducted on both scaffolds' top. The scanned area was 1000 × 500 μm^2 to perform a proper set of measurement indicated in Fig. 7 with a red dotted line of 1 mm.

For scaffold (A) — fabricated to map the effects of various repetition rates — the outer ring, the inner ring and the cylindrical core were cured with 5 Hz, 20 Hz and 50 Hz, respectively, while the fluence per pulse was kept constant at 15 mJ/cm^2.

With scaffold (B) — built to evaluate the effects of different laser pulse fluences — the outer ring, the inner ring, and the core were cured at 5 mJ/cm^2, 15 mJ/cm^2 and 25 mJ/cm^2, keeping the repetition rate at constant 20 Hz.

Nanoindentation results show that the stiffness of each segment is clearly different from the other two in both constructs (Fig. 7). On scaffold (A), the mean value of the Young's modulus is 85 MPa, 135 MPa and 165 MPa for the segment fabricated with 50 Hz, 20 Hz and 5 Hz, respectively, suggesting a clear tuning relation between the stiffness and the repetition rate in the investigated frequency range. Local extremes are observed at the boundaries of the overlapping segments. For scaffold (B), the mean value is less than 5 MPa for the core (25 mJ/cm^2), 130 MPa for the inner ring (15 mJ/cm^2) and 450 MPa for the outer (5 mJ/cm^2), showing that decreasing the fluence drastically increases the stiffness. Local extremes mentioned previously on scaffold (A) were not detected. This could be explained by the greater difference between the segments' mechanical properties.

The stiffness behavior of the two constructs presented in Fig. 7 shows similarity to the composite scaffolds used for tissue interface regeneration [25–29], albeit fabricated from the same biodegradable biocompatible material. Since the segments' porosities could be adjusted with proper masking, these scaffolds are potentially ideal for cartilage repair or dermal tissue regeneration.

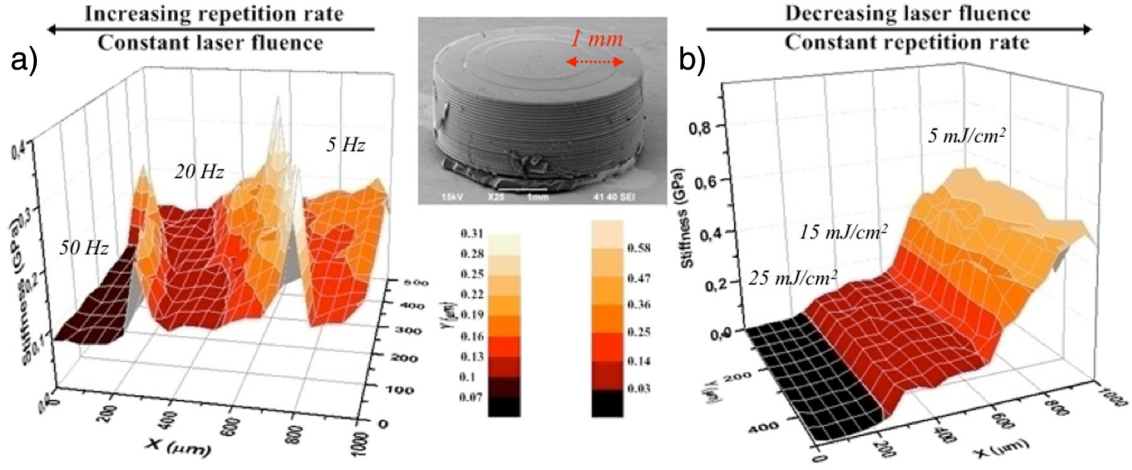

Fig. 7. Scaffold with 3 different regions due to various laser parameters: (a) repetition rate changed, and (b) fluence per pulse changed. The small inset photo on the center displays the real scaffold analyzed.

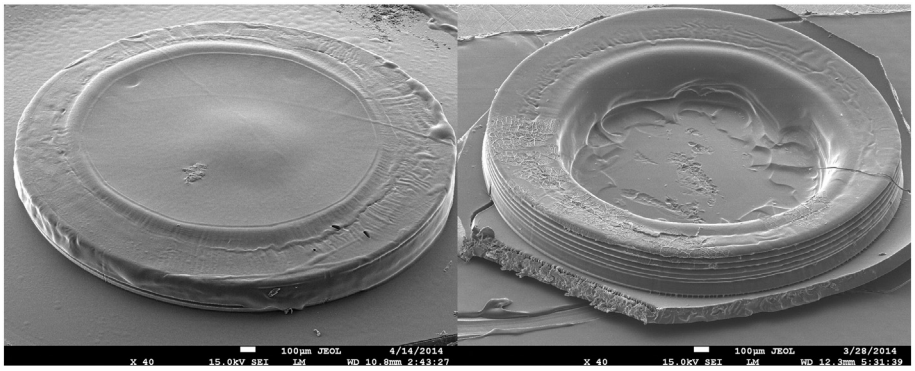

Fig. 8. Degradation of a multi-phase segmented scaffold before (on the left) and after soaking (on the right) in DMEM for 7 days at 37 °C. The core area completely disappeared while the rim remained intact for another 14 days.

3.3.2. Multi-phase degradation scaffolds

From the considerations on the relationship between mechanical properties and network structure, we deduce that the stiffness-tuning also leads to different degradation properties. Thus, multi-phase degradation scaffolds can be fabricated where certain areas will degrade quicker than others. Such constructs can be useful for controlled vascularization of the regenerating tissue.

To exhibit the multiphase degradation, a simple dual-segmented construct was produced. The core was fabricated with a higher fluence (25 mJ/cm^2) and repetition rate (100 Hz) in contrast to the rim (10 mJ/cm^2, 5 Hz).

After soaking the sample for 7 days in 37 °C DMEM, the core area degraded and disappeared while the rim remained intact (Fig. 8). The rim did not degrade for another 14 days.

4. Conclusions

The MPExSL process is capable of producing structures with different geometries, sizes, and porosities from a liquid UV-curable resin. The physical properties of these structures are affected by the photoinitiator concentration and various irradiation conditions.

We showed that by merely changing two laser parameters (the repetition rate and the fluence per pulse), MPExSL scaffold's stiffness could be tuned in four orders (4 MPa–4 GPa). This facile, *in situ* large-scale tuning capability is a great asset of the MPExSL technique. We demonstrated the utility of the constructs with localized physical properties fabricated from a single resin composition. This wide range tuning capability will potentially lead to new directions in scaffold design and facilitate the multiphase scaffold production.

Acknowledgments

This work has received funding support from the European Union (FP7-NMP-2013-EU-China) grant agreement no. 604263 (NEUROSCAFFOLDS). Ms. Lara Marini is acknowledged for the TGA and DSC measurements.

References

[1] R. Langer, J.P. Vacanti, Tissue engineering, Science 260 (1993) 920–926, http://dx.doi.org/10.1126/science.8493529.
[2] Y. Tabata, Biomaterial technology for tissue engineering applications, J. R. Soc. Interface 6 (2009) S311–S324, http://dx.doi.org/10.1098/rsif.2008.0448.focus.
[3] H. Liu, X. Ding, G. Zhuo, P. Li, X. Wei, Y. Fan, Electrospinning of polymeric nanofibers for tissue engineering applications: a review, Tissue Eng. 12 (5) (2006) 1197–1211, http://dx.doi.org/10.1155/2013/495708.
[4] D.W. Hutmacher, Scaffolds in tissue engineering bone and cartilage, Biomaterials 21 (2000) 2529–2543, http://dx.doi.org/10.1016/S0142-9612(00)00121-6.
[5] S.J. Hollister, Scaffold design and manufacturing: from concept to clinic, Adv. Mater. 21 (2009) 3330–3342, http://dx.doi.org/10.1002/adma.200802977.
[6] B.A. Harley, A.K. Lynn, Z. Wissner-Gross, W. Bonfield, I.V. Yannas, L.J. Gibson, Design of a multiphase osteochondral scaffold III: fabrication of layered scaffolds with continuous interfaces, J. Biomed. Mater. Res. Part A 92 (2010) 1078–1093, http://dx.doi.org/10.1002/jbm.a.32387.
[7] C. Wei, L. Cai, B. Sonawane, S. Wang, J. Dong, High-precision flexible fabrication of tissue engineering scaffolds using distinct polymers, Biofabrication 025009 (2012), http://dx.doi.org/10.1088/1758-5082/4/2/025009.
[8] S. Beke, B. Farkas, I. Romano, F. Brandi, 3D scaffold fabrication by Mask Projection Excimer Laser Stereolithography, Opt. Mater. Express 4 (10) (2014) 2032–2041, http://dx.doi.org/10.1364/OME.4.002032.
[9] S. Beke, F. Anjum, H. Tsushima, L. Ceseracciu, E. Chieregatti, A. Diaspro, A. Athanassiou, F. Brandi, Towards excimer-laser-based stereolithography: a rapid process to fabricate rigid biodegradable photopolymer scaffolds, J. R. Soc. Interface 76 (2012) 3017–3026, http://dx.doi.org/10.1089/107632701753337645.
[10] B. Farkas, A. Zsedenyi, E. Gyukity-Sebestyen, I. Romano, K. Nagy, Alberto Diaspro, F. Brandi, K. Buzas, S. Beke, Excimer laser-produced biodegradable photopolymer scaffolds do not induce immune rejection in vivo, J. Laser Micro/Nanoeng (2015), http://dx.doi.org/10.2961/jlmn.2015.01.0001.
[11] S. Scaglione, R. Barenghi, S. Beke, L. Ceseraccio, I. Romano, F. Sbrana, P. Stagnaro, F. Brandi, M. Vassali, Characterization of bioinspired elastin-polypropylene fumerate material for vascular prostheses applications, SPIE Opt. Metrol. 6 (2013), http://dx.doi.org/10.1117/12.2021754 (87920H-87920H).
[12] Rossella Barenghi, Szabolcs Beke, Ilaria Romano, et al., Elastin-coated biodegradable photopolymer scaffolds for tissue engineering applications, Biomed. Res. Int. 2014 (2014), http://dx.doi.org/10.1155/2014/624645 (Article ID 624645, 9 pp.).
[13] S. Beke, L. Kőrösi, A. Scarpellini, F. Anjum, F. Brandi, Titanate nanotube coatings on biodegradable photopolymer scaffolds, Mater. Sci. Eng. C 33 (2013) 2460–2463, http://dx.doi.org/10.1016/j.msec.2013.01.066.
[14] S. Beke, R. Barenghi, B. Farkas, I. Romano, L. Kőrösi, S. Scaglione, F. Brandi, Improved cell activity on biodegradable photopolymer scaffolds using titanate nanotube coatings, Mater. Sci. Eng. C (2014), http://dx.doi.org/10.1016/j.msec.2014.07.008.
[15] Photoinitiators for UV Curing: Formulator's Guide for CoatingsCiba, http://www.mufong.com.tw/Ciba/ciba_guid/photo_uv_2.pdf.
[16] J.P. Fisher, M.D. Timmer, T.A. Holland, D. Dean, P.S. Engel, A.G. Mikos, Photoinitiated cross-linking of the biodegradable polyester poly(propylene fumarate). Part I. Determination of network structure, Biomacromolecules 4 (2003) 1327–1334, http://dx.doi.org/10.1021/bm030028d.
[17] A.G. Mikos, C.G. Takoudis, N.A. Peppas, Kinetic modeling of copolymerization/crosslinking reactions, Macromolecules 19 (1986) 2174–2182, http://dx.doi.org/10.1021/ma00162a012.
[18] M.D. Timmer, S. Jo, C. Wand, C.G. Ambrose, A.G. Mikos, Characterization of the cross-linked structure of fumarate-based degradable polymer networks, Macromolecules 5 (2002) 4373–4379, http://dx.doi.org/10.1021/ma020028q.
[19] L. Holiday, J.W. White, The stiffness of polymers in relation to their, structure, http://pac.iupac.org/publications/pac/pdf/1971/pdf/2603x0545.pdf.
[20] R. Brown, Handbook of Polymer Testing, CRC Press 1999, p. 202.
[21] R.G. Wells, The role of matrix stiffness in regulating cell behavior, Hepatology 47 (2008), (http://onlinelibrary.wiley.com/doi/10.1002/hep.22193/pdf).
[22] B.N. Mason, J.P. Califano, C.A. Reinhart-King, Matrix stiffness: a regulator of cellular behavior and tissue formation, Eng. Biomater. Regen. Med. (2012) 19–37, http://dx.doi.org/10.1007/978-1-4614-1080-5_2 (book chapter).
[23] A. Haage, I.C. Schneider, Cellular contractility and extracellular matrix stiffness regulate matrix metalloproteinase activity in pancreatic cancer cells, FASEB J. (2014), http://dx.doi.org/10.1096/fj.13-245613 fj.13-245613.
[24] R.S. Fischer, K.A. Myers, M.L. Gardel, C.M. Waterman, Stiffness-controlled three-dimensional extracellular matrices for high-resolution imaging of cell behavior, Nat. Protoc. 7 (2012) 2056–2066, http://dx.doi.org/10.1038/nprot.2012.127.
[25] J.K. Sherwood, S.L. Riley, R. Palazzolo, S.C. Brown, D.C. Monkhouse, M. Coates, L.G. Griffith, L.K. Landeen, A. Ratcliffe, A three-dimensional osteochondral composite scaffold for articular cartilage repair, Biomaterials 23 (2002) 4739–4751, http://dx.doi.org/10.1016/s0142-9612(02)00223-5612.
[26] P. Nooeaid, V. Salih, J.P. Beier, A.R. Boccaccini, Osteochondral tissue engineering: scaffolds, stem cells and applications, J. Cell. Mol. Med. 16 (2012) 2247–2270, http://dx.doi.org/10.1111/j.1582-4934.2012.01571.x.
[27] A.K. Lynn, S.M. Best, R.E. Cameron, B.A. Harley, I.V. Yannas, L.J. Gibson, W. Bonfield, Design of a multiphase osteochondral scaffold. I. Control of chemical composition,

J. Biomed. Mater. Res. Part A 92 (2010) 1057–1065, http://dx.doi.org/10.1002/jbm.a.32415.
[28] H. Zhao, G. Wang, S. Hu, J. Cui, N. Ren, D. Liu, H. Liu, C. Cao, J. Wang, Z. Wang, In vitro biomimetic construction of hydroxyapatite-porcine acellular dermal matrix composite scaffold for MC3T3-E1 preosteoblast culture, Tissue Eng. Part A 17 (5–6) (2011) 765–776, http://dx.doi.org/10.1089/ten.TEA.2010.0196.
[29] S.P. Zhong, Y.Z. Zhang, C.T. Lim, Tissue scaffolds for skin wound healing and dermal reconstruction, Wires Nanomed. Nanobiotechnol. (2010), http://dx.doi.org/10.1002/wnan.100.
[30] S. Beke, F. Anjum, L. Ceseracciu, I. Romano, A. Athanassiou, A. Diaspro, F. Brandi, Rapid fabrication of rigid biodegradable scaffolds by excimer laser mask projection technique: a comparison between 248 and 308 nm, Laser Phys. 23 (3) (2013) 035602, http://dx.doi.org/10.1088/1054-660X/23/3/035602.
[31] K.F. Kasper, K. Tanahashi, J.P. Fisher, A.G. Mikos, Synthesis of poly(propylene fumarate), Nat. Protoc. 4 (2009) 518–525, http://dx.doi.org/10.1038/nprot.2009.24.
[32] P.X. Lan, J.W. Lee, Y.J. Seol, D.W. Cho, Development of 3D PPF/DEF scaffolds using micro-stereolithography and surface modification, J. Mater. Sci. Mater. Med. 20 (2009) 271–279, http://dx.doi.org/10.1007/s10856-008-3567-2.
[33] F. Brandi, F. Anjum, L. Ceseracciu, A.C. Barone, A. Athanassiou, Rigid biodegradable photopolymer structures of high resolution using deep-UV laser photocuring, J. Micromech. Microeng. 21 (2011), http://dx.doi.org/10.1088/0960-1317/21/5/054007.
[34] S. Wang, M.J. Yaszemski, J.A. Gruetzmacher, L. Lu, Photo-crosslinked poly(ε-caprolactone fumarate) networks: roles of crystallinity and crosslinking density in determining mechanical properties, Polymer (Guildf) 49 (2008), http://dx.doi.org/10.1016/j.polymer.2008.10.021.